Journal of Magnetism and Magnetic Materials 541 (2022) 168525

Contents lists available at ScienceDirect

Journal of Magnetism and Magnetic Materials

journal homepage: www.elsevier.com/locate/jmmm

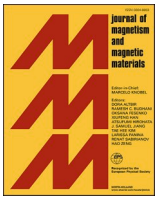

Magnetic correlations peculiarities in amorphous Fe-Cu-Nb-Si-B alloy ribbons

N.V. Ilin [a,*], S.V. Komogortsev [b], G.S. Kraynova [a], A.V. Davydenko [a], I.A. Tkachenko [c], A. G. Kozlov [a], V.V. Tkachev [a], V.S. Plotnikov [a]

[a] Far Eastern Federal University, 690922 Vladivostok, Russia
[b] Kirensky Institute of Physics, Federal Research Center KSC SB RAS, 660036 Krasnoyarsk, Russia
[c] Institute of Chemistry, FEB RAS, 690022 Vladivostok, Russia

ARTICLE INFO

Keywords:
Amorphous alloys
Magnetic correlations
Random magnetic anisotropy
X-ray diffraction
Exchange stiffness constant
Kerr microscopy

ABSTRACT

Understanding the magnetic correlations in amorphous alloys is the key to enhancing their high soft magnetic properties. The magnetization correlations were studied in amorphous alloy ribbons Fe-Cu-Nb-Si-B by analysis of approach to magnetic saturation within the random magnetic anisotropy model. An unusual sequence of power laws during approach of the magnetization to saturation was observed. This may indicate the transition from isotropic to anisotropic magnetic correlations as the applied field decreases.

1. Introduction

Nanocrystalline and amorphous magnetic alloys are of interest due to the excellent soft magnetic properties. The nanocrystalline Finemet-type alloys annealed from the amorphous Fe-Cu-Nb-Si-B precursor are used in transformers and chokes, electromagnetic screens, and electromagnetic interference filters because of prosperous combination of the electrical and magnetic properties [1,2]. However, a detailed study of the structural relaxation processes and the changes in the magnetic properties during the transformation of an amorphous alloy into a nanocrystalline one is impossible without studying the structural and magnetic state of the amorphous precursor. This information is the important point for the study of nanocrystalline magnets.

The relationship between structure and properties in amorphous and nanocrystalline alloys is well described within the random magnetic anisotropy (RMA) model [3,4]. This makes the RMA model useful for designing new amorphous and nanocrystalline alloys and improving properties of the existing ones [4–6]. The RMA model explains the origin of key advantage of these alloys: the extremely high magnetic softness.

The lack of long-range order in amorphous alloy results in disappearance of its macroscopic crystallographic magnetic anisotropy. However, some short-range order and the local deviations in the ideal glass structure lead to the local magnetic anisotropy appearance with the energy constant K_{local} and randomly oriented easy magnetization axis [3,4]. The scale within which the local easy axis is ordered is referred to as a structural correlation length L_C. In the amorphous alloys, there is disorder of magnetization direction at macroscale either but there is the ferromagnetic order within the magnetic correlation length L_H. Averaging of the anisotropy within the magnetic correlation volume provides a proper explanation and description of soft magnetic properties of amorphous and nanocrystalline alloys [4,6]. In this regard, measuring the magnetic correlation length is very important for understanding the relationship between the structure and properties of these alloys. The magnetic correlation length is measured by Kerr, Lorentz and magnetic force microscopies [7–9]. These techniques record the magnetic microstructure on a sample surface. Two methods are currently used for the measurement the magnetic correlation length in the sample volume: the small angle neutron scattering [10] and the correlation magnetometry method based on the analysis of approaching to the magnetic saturation [11]. The correlation magnetometry method makes it possible to measure not only the magnetic correlation length, but also the averaged magnetic anisotropy, which is the main clue to understanding their magnetic softness. The fundamentals of correlation magnetometry are theoretical expressions for magnetic correlation function parameters: a variance of the magnetization component transverse to the applied field and the magnetic correlation length [6,11–15].

In this work we studied the magnetic correlations of rapidly

* Corresponding author.
E-mail address: ilin_nva@dvfu.ru (N.V. Ilin).

https://doi.org/10.1016/j.jmmm.2021.168525
Received 18 February 2021; Received in revised form 30 August 2021; Accepted 3 September 2021
Available online 7 September 2021
0304-8853/© 2021 Elsevier B.V. All rights reserved.

quenched Fe-Cu-Nb-Si-B alloys of various composition by the correlation magnetometry method and provided a comparative analysis of their magnetic and structural characteristics.

2. Experiment

The Fe-Cu-Nb-Si-B ribbons were produced by melt spinning technique, which consists in ultrafast quenching of an amorphous metal ribbon on the surface of a rotating cooler drum (cooling rate was about 10^6 K/s). The thickness of the ribbons was about 20 μm. Ribbons of three Finemet-type compositions were studied: $Fe_{74.3}Cu_{0.2}Nb_3Si_{16.5}B_6$, $Fe_{74}Cu_1Nb_3Si_{16}B_6$ and $Fe_{73}Cu_{1.5}Nb_3Si_{16.5}B_6$. The composition of finemet-type alloys is optimized for all components, including copper [5,16,17]. Small variations relative to this optimal composition reserve a general set of features inherent in the alloy but can strongly affect a particular characteristic (for example, coercivity or magnetization) and the structural state. The compositions selected for our study meet this condition of the small composition variation relative to the optimal one for finemet-type alloys.

The magnetization curves were measured using a magnetometer PPMS 9 T Quantum Design in field up 9 T (7160 kA/m); the magnetization behavior at low-temperatures was studied with a SQUID-magnetometer MPMS 7XL Quantum Design.

To control the demagnetizing field, the samples were prepared in the shape of thin disks with a diameter of 3.7 ÷ 3.9 mm. The demagnetizing factor N_a (for the applied field along the ribbon plane) was calculated using the equation for an oblate ellipsoid of revolution in the limit $\alpha = c/a = \frac{0.02[mm]}{D[mm]} \ll 1$ [18] and it was in the range $N_a \approx 0.0040 \div 0.0042$ for the three measured samples. To further analysis the values of applied field were corrected using the demagnetizing field estimated as $M{\cdot}N_a$ and was up to 3 ÷ 4 kA/m.

The magnetic domain structure was studied using a magneto-optical Kerr microscope Evico Magnetics GmbH. Both the magnetic domain patterns and the magnetization curves were recorded in the field applied along the ribbon plane and transverse the rolling axis. X-ray diffraction was measured with a diffractometer Bruker D8 Advance using Cu-Kα radiation (the wavelength was λ = 1.5406 Å).

3. Theory

3.1. Correlation magnetometry

The main value to be compared with the theoretical one in correlation magnetometry method is the variance of the transverse to the field magnetization component ν_m. The magnetization near saturation is related to ν_m as:

$$M(H) = M_S(1 - \nu_m(H)) \tag{1}$$

here M_S is saturation magnetization. This allows us to estimate ν_m from the magnetization curve in the region of approaching to saturation [12,13]: $\nu_m = \frac{M_S - M(H)}{M_S}$. Due to the competition of the random local anisotropy and the applied field, the magnetization would approach total saturation in an infinite field limit.

In the strong field there is no magnetic domains and magnetization vector deviates slightly from the field direction. In this case magnetization approaches to saturation reversibly and follows to a specific law. According to the random anisotropy model the magnetization variance is given by [14,15]:

$$\nu_m = \frac{aL_H}{4\pi\delta^4}\int C(\vec{r})e^{-r/L_H}d^3r \tag{2}$$

here a is a symmetry coefficient equal to 1/15; $\delta = \sqrt{A/K_{local}}$; $C(\vec{r})$ is the correlation function of the local easy magnetization axis; $L_H = \sqrt{\frac{2A}{\mu_0 M_S H}}$ is a ferromagnetic correlation length (or the magnetization ripple length);

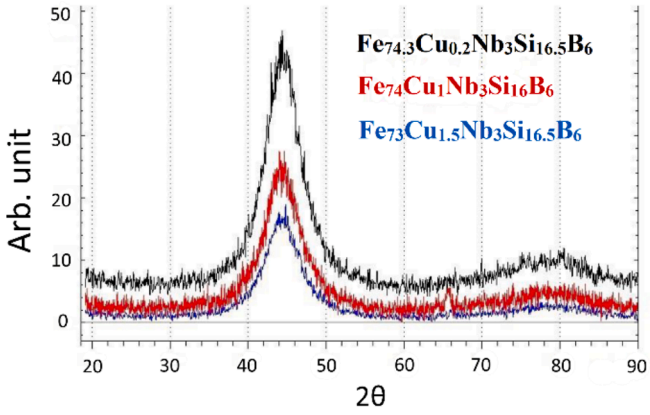

Fig. 1. X-ray powder diffraction pattern of Fe-Cu-Nb-Si-B ribbon.

A is an exchange stiffness constant. The question of the specific functional dependence of the $C(\vec{r})$ in an amorphous alloy remains open. For example, it can be assumed that type $C(\vec{r})$ can differ for various alloys [19]. The universal assumption for the function $C(\vec{r})$ is that it will tend to zero for the distances r greater than L_C. In this case, only the length L_C, at which the correlations of the easy axis become vanishing, matters only. The two limits corresponding to the cases $L_H \ll L_C$ and $L_H \gg L_C$ lead to two asymptotic modes of Eq. (2):

$$\nu_m = \begin{cases} \dfrac{aH_a^2}{H^2}, \ for\ L_H \ll L_C, H \gg H_L \\ \dfrac{aH_a^2}{H^{d/2}H_L^{(4-d)/2}}, \ for\ L_H \gg L_C, H \ll H_L \end{cases} \tag{3}$$

where d is a dimension of ferromagnetic correlations, $H_L = 2A/\mu_0 M_S L_C^2$ is a correlation field, $H_a = \frac{2K_{local}}{\mu_0 M_S}$ is a field of local magnetic anisotropy.

For the limit of strong field ($L_H \ll L_C, H \gg H_L$), the asymptotic mode provides well known Akulov's law [5] for non-interacting particles. According to [20–23] for ferromagnets at finite temperature and in strong magnetic field, it is necessary to take into account the contribution to magnetization linearly increased with the field. Therefore, in Akulov's law (Eq. (3)) (for fields above 20 kA/m) the high-field component χH should be added, which leads to the following form of the law of approach the magnetization to saturation:

$$M = M_S\left(1 - \frac{aH_a^2}{H^2}\right) + \chi H \tag{4}$$

Also, the exponent in the power dependence $\nu_m \propto H^n$ corresponding to Eq. (3) can differ in various materials in low-field mode ($L_H \gg L_C, H \ll H_L$), since related to the fractal dimension d of the magnetic correlation volume $V_H \propto L_H^d$ packed with correlated easy axis volumes V_C [24].

Using log–log scale is a convenient way to analyze the power-law behavior since any power-law dependence will be visualized as a straight line, and its slope will provide the exponent. We will use this approach to analyze the power-law behavior of magnetization variance. The power-law exponent is n = -2 for the high-field regime according to Eq. (3) (strong field limit) and n = -1, −1/2 for the medium-field regime. In the last case its value depends on the dimensionality of the magnetic correlation volume or the dimensionality of the magnetic anisotropy heterogeneity [11,25–29].

4. Results

4.1. Atomic structure

The broad diffuse peaks on the X-ray diffraction profiles (Fig. 1) indicate that the studied Fe-Cu-Nb-Si-B alloys are amorphous. Some

Table 1
Structural parameters of Fe-Cu-Nb-Si-B alloys.

Alloy composition	Scattering angle 2θ, deg.	Bragg's spacing d, nm	β, deg.	τ, nm
Fe74.3Cu0.2Nb3Si16.5B6	44.5	0.204	5.5 ± 0.5	1.54 ± 0.19
Fe74Cu1Nb3Si16B6	44.5	0.204	5.5 ± 0.4	1.54 ± 0.15
Fe73Cu1.5Nb3Si16.5B6	44.5	0.204	4.7 ± 0.8	1.79 ± 0.30

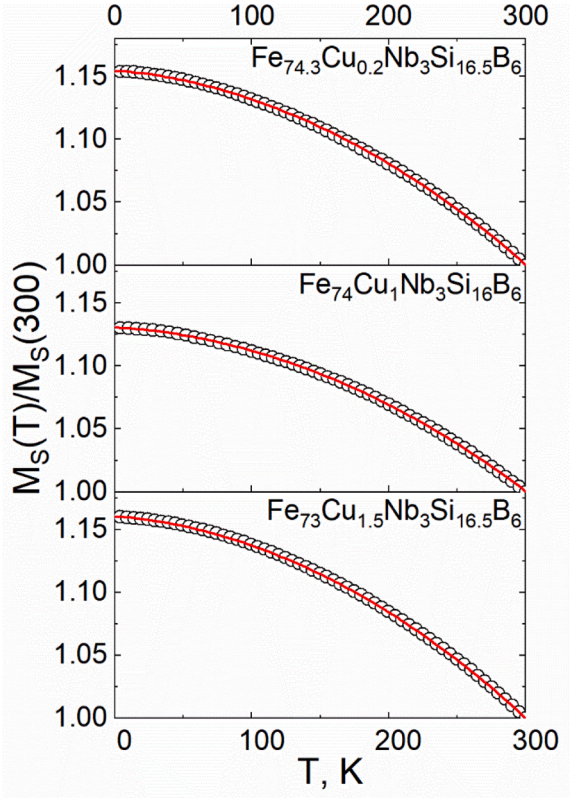

Fig. 2. Thermal variation of the magnetization of amorphous alloy ribbons Fe-Cu-Nb-Si-B in the temperature range of 5 ÷ 300 K: circles are experimental points, solid line is a fitting line with Bloch's law.

estimate of short-range order was carried out by the Scherrer equation for the coherent scattering length [30]:

$$\tau = \frac{180}{\pi}\frac{0.89\lambda}{cos(\theta)\beta} \quad (5)$$

where λ is the used X-ray wavelength, θ is the Bragg angle, and β is the peak width at half of the maximum intensity. The results of the X-ray pattern analysis are collected in the Table 1.

4.2. Magnetic constants

The exchange stiffness constant was estimated using the analysis of

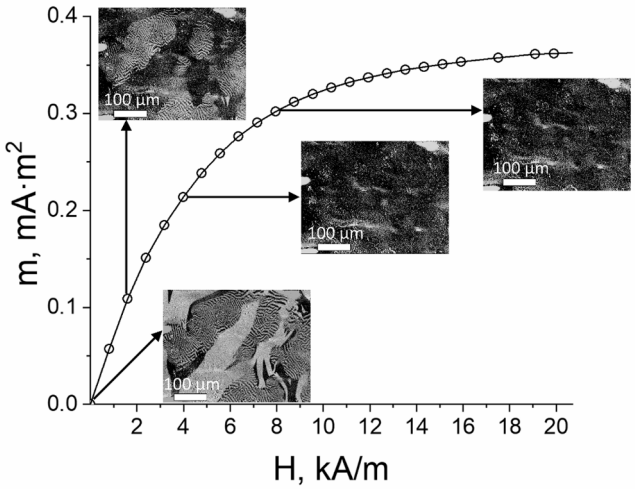

Fig. 3. Dependence of the magnetic moment on the magnetic field in amorphous ribbons Fe-Cu-Nb-Si-B. Domain structures in corresponding magnetic fields are shown in the insets.

low-temperature magnetization behavior within Bloch's law $T^{3/2}$ [31]:

$$\frac{M_S(T)}{M_S(0)} = 1 - BT^{3/2} - CT^{5/2} + O(T^{7/2}) \quad (6)$$

Here B is the Bloch constant, which is directly related to the exchange stiffness constant A [31,32]:

$$A = \frac{k_B}{8\pi}\left(\frac{M_S(0)}{g\mu_B}\right)^{1/3}\left(\frac{\zeta(3/2)}{B}\right)^{2/3} \quad (7)$$

where $g = 2.1$ is the Landé g-factor, μ_B is the Bohr magneton, k is the Boltzmann constant, $\zeta(3/2) = 2.612$ is the Riemann zeta function at 3/2. The fitting of low-temperature magnetization behavior with Eq. (7) is highly reliable (see Fig. 2) and the best fitting parameters along with estimated exchange stiffness constants are outlined in Table 2. The saturation magnetization M_S at room temperature measured using the ferromagnetic resonance in [33] is also presented in Table 2.

4.3. Magnetization curve

The studied Fe-Cu-Nb-Si-B ribbons demonstrate soft magnetic properties (coercivity $H_C \approx 24$ A/m) that is common feature for majority of amorphous alloys of similar composition. The law of approach to magnetic saturation is valid only for strong enough applied fields that at least correspond to a reversible part of magnetization curve. The reversible magnetic response is valid in the fields where the magnetic domain structure has disappeared. We evaluated this lower border field using a Kerr microscope. The magnetic domain patters corresponded to different parts of magnetization curve are shown in Fig. 3.

Below 1.6 kA/m the domain patterns of two types were observed in the magnetic contrast images which are common for the amorphous alloy ribbons [34,35]. The patterns of the first type consist of domains with the in-plane magnetization and the ones of the second type are include the labyrinth-type narrow domains (fingerprint patterns). The observed fingerprints are the closure structure of the volume domains with the magnetization oriented perpendicular to the plane of the

Table 2
Fitting parameters of Bloch's Law $T^{3/2}$ and magnetic constants of Fe-Cu-Nb-Si-B alloys.

Alloy composition	B, 10^{-5} $K^{-3/2}$	C, 10^{-8} $K^{-5/2}$	$\sigma_S(0)$, A·m^2 kg^{-1}	$\mu_0 M_S$ (room temp.), T	$\mu_0 M_S(0)$, T	A, 10^{-12} J·m^{-1}
$Fe_{74.3}Cu_{0.2}Nb_3Si_{16.5}B_6$	1.69	2.90	145 ± 4	1.13 ± 0.03	1.30 ± 0.03	5.95 ± 0.05
$Fe_{74}Cu_1Nb_3Si_{16}B_6$	1.33	2.94	150 ± 4	1.21 ± 0.03	1.37 ± 0.04	7.10 ± 0.08
$Fe_{73}Cu_{1.5}Nb_3Si_{16.5}B_6$	1.61	3.48	140 ± 5	1.02 ± 0.03	1.19 ± 0.03	5.94 ± 0.06

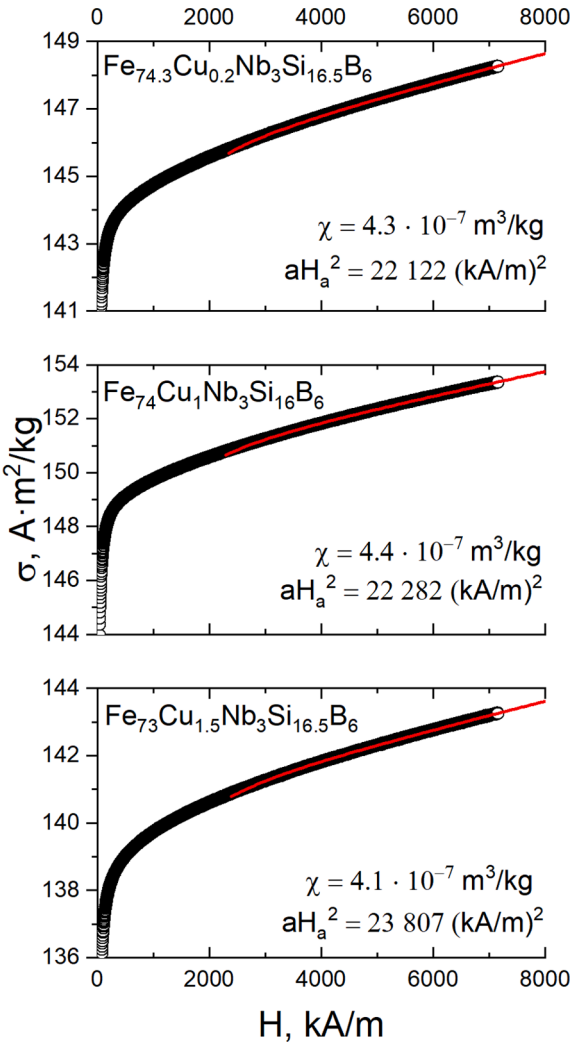

Fig. 4. Approach magnetization to saturation in Fe-Cu-Nb-Si-B ribbons. Circles are experimental points; solid line is a fitting line with Akulow's law (Eq. (4)).

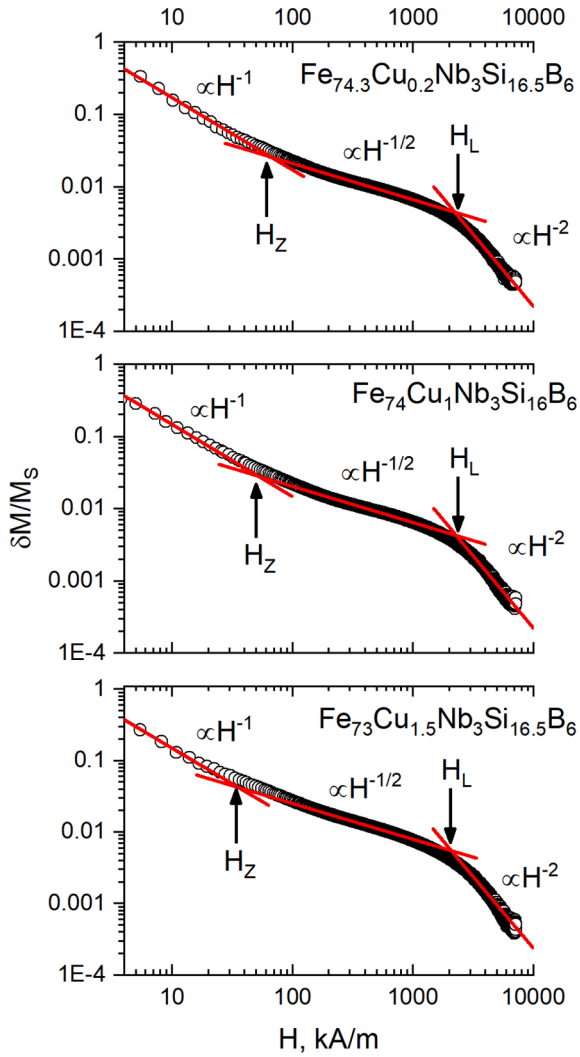

Fig. 5. The magnetization variance versus magnetic field in amorphous ribbons Fe-Cu-Nb-Si-B (1column).

Table 3
Correlation parameters of Fe-Cu-Nb-Si-B alloys.

Alloy composition	H_a, kA·m^{-1}	H_L, kA·m^{-1}	H_Z, kA·m^{-1}	K_{local}, 10^5 J·m^{-3}	L_C, nm	L_Z, nm
$Fe_{74.3}Cu_{0.2}Nb_3Si_{16.5}B_6$	576	2228	66	3.6 ± 0.1	2.1 ± 0.1	12
$Fe_{74}Cu_1Nb_3Si_{16}B_6$	578	2290	52	3.5 ± 0.1	2.3 ± 0.1	15
$Fe_{73}Cu_{1.5}Nb_3Si_{16.5}B_6$	598	2084	36	3.1 ± 0.1	2.4 ± 0.1	18

ribbons. The perpendicular magnetic anisotropy in the regions with fingerprints is induced by in-plane compressive stresses [35–37]. It was found that in the Fe-Cu-Nb-Si-B ribbons the in-plane domain patterns disappear in fields above 1.6 kA/m, while the fingerprint patterns disappear in fields above 4.8 ÷ 5.6 kA/m. The last values provide a bottom estimate for the fields to be used for analysis of the approaching to the magnetic saturation.

Approaching to magnetic saturation part of *M(H)* in the ribbons (Fig. 4) is the result from competition of the magnetization fluctuations due to the random orientation of the local easy axis and applied uniform field and also high-field linear contribution. In the strong fields, above 3000 kA/m *M(H)* was very well fitted with Eq. (4). The local anisotropy fields H_a and local anisotropy constant K_{local} were estimated using fitting by Eq. (4) for this part of *M*(*H*) curve and are summarized in Table 3. The values of K_{local} in Table 3 significantly exceed the anisotropy constant K_1 of crystalline iron and iron-silicon alloys [38,39]. Such a high value of K_{local} is apparently characteristic of amorphous alloys and were discussed in [28], there was argued that in amorphous iron-based alloys local anisotropy constant can reach up to 10^6 J/m^3. According to [28], a higher local magnetic anisotropy constant may results from the cubic symmetry destruction of the nearest surroundings of crystalline iron. In addition, local elastic stresses in the amorphous alloy contribute to the value of local anisotropy constant, taking into account the fact that the magnetostriction constant in amorphous alloys of similar composition is positive and large enough in comparison with the constant of nanocrystalline alloys [4,5,35].

For further analysis of nonlinear power-law behavior of the approach to magnetic saturation, we subtracted the contribution of the linear component: $M(H) \rightarrow M(H) - \chi H$.

5. Discussion

The field behavior of the magnetization variance follows three power-laws in different field ranges for the Fe-Cu-Nb-Si-B alloy ribbons

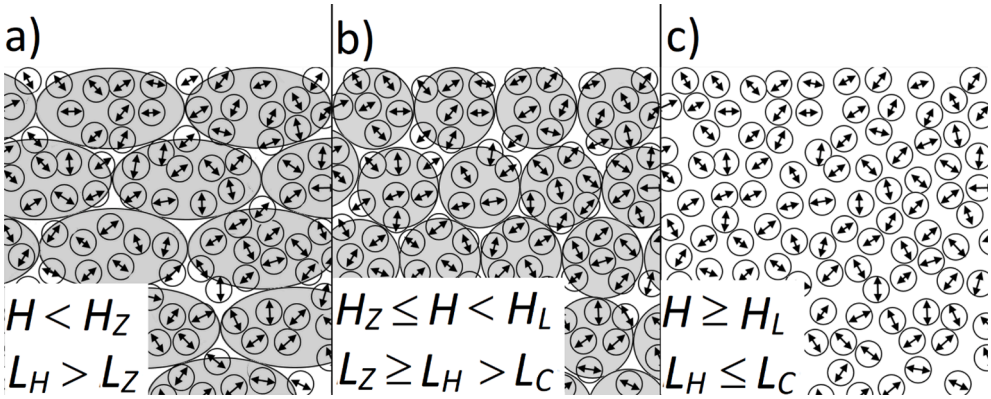

Fig. 6. Schematic representation of magnetic correlations in amorphous Fe-Cu-Nb-Si-B ribbons in different field ranges: a) low-field regime, anisotropic magnetic correlations; b) medium-field regime, isotropic magnetic correlations; c) high-field regime, magnetic correlation within structural correlations.

(Fig. 5). A power-law with the exponent n = -2 (Akulov's law Eq. (3)), was observed in strongest fields. In the medium fields $H < H_L$ the curve of approaching magnetization to saturation follows a power-law $\delta M(H)/M_S \propto H^{-1/2}$. The transition at $H = H_L$ is expected within the RMA model and is frequently observed in the experiment [6,12,14,40,41]. The explanation of the transition is as follows. As the field decreases below H_L, the magnetic correlation length L_H is grown in isotropic manner and covers a number of structural correlation volumes V_C. Averaging the local magnetic anisotropy constant K_{local} within such an isotropic magnetic correlation volume according to the RMA model [3,4] lead to the appearance of average anisotropy constant $\langle K \rangle = \frac{K_{local}}{\sqrt{N}}$, that provides magnetization variance behavior as $v_m \propto H^{-1/2}$ [28,42,43]. The observation of transition between different power laws using log–log plots provides the correlation field H_L as a crossover point of the lines corresponded to $\delta M(H)/M_S \propto H^{-1/2}$ and $\delta M(H)/M_S \propto H^{-2}$ regimes [44,45]. The H_L fields estimated in this way are summarized in Table 3.

In the log–log plot the unusual transition was observed in the low fields: the behavior with applied field decreasing from the medium field regime reveals the power-law transition from one with exponent $n = -1/2$ to that $n = -1$ (Fig. 5). The fact of power-law behavior $\delta M(H)/M_S \propto H^{-1}$ observation in Fig. 5 at low fields looks reliable. A power law with exponent $n = -1$ has observed and discussed for amorphous alloy ribbons [23,28,46] but the sequence of power laws similar as to observed in our study had not been observed earlier. An explanation of such transition may be a change in the growth mode of magnetic correlation volume with field decreasing from isotropic (in medium fields) to anisotropic in low fields. The mechanism of the observed transitions in power-law regimes of magnetization variance is sketched in Fig. 6.

The isotropic growth mode implies dimension of the magnetic correlation volume to be $D = 3$ (at the medium fields there $L_H > L_C$) and therefore the power-law regime with the exponent $n = -1/2$ is observed (see Eq. (3) and Fig. 6 (b)). The anisotropic growth mode may be related with the dimension of magnetic correlation volume $D = 2$ and the power-law regime with the n = -1 (see Eq. (3) and Fig. 6 (a)). In the strong applied fields ($L_H < L_C$), the magnetization approaches to the saturation according to Akulov's law (see Eq. (3) and Fig. 6 (c)). The transition between power-law from one with exponent $n = -1/2$ (isotropic magnetic correlations with D = 3) to that with $n = -1$ (anisotropic magnetic correlations with D = 2) occurs at a certain magnetic correlation length L_Z and at a certain applied field H_Z observed in Fig. 5. The data on H_Z and L_Z are ummarized in Table 3.

The structural correlation length in Fe-Cu-Nb-Si-B ribbons according to Table 3 is $L_C \approx 2.3$ nm, which is about 9 interatomic distances. The coherent scattering length τ (Table 1) is about 6 interatomic distances which is 1.5 times less than the structural correlation length L_C. Let us note that and L_C in any case are close in order of magnitude. The coherent scattering length provides the lowest boundary of the ordering scale. Additionally, the intrinsic stresses in the rapidly quenched alloy [22,23] increase the FWHM of X-ray diffraction peak, and as a result reduce the estimated coherent scattering length [47].

6. Conclusions

Magnetization correlations of rapidly quenched Fe-Cu-Nb-Si-B alloy ribbons are studied using the correlation magnetometry. The collapse fields of the domain structure estimated using a Kerr microscopy provide a bottom estimate for the fields used for analysis of the magnetization curves in the region of approaching to the magnetic saturation. The local magnetic anisotropy constants are calculated by fitting magnetization curve in strong fields (upper 3000 kA/m) with Akulov's law. In fields from 80 to 2000 kA/m the approach to magnetic saturation follows $\delta M(H)/M_S \propto H^{-1/2}$ dependence, which corresponds to the isotropic magnetic correlation volumes V_H (dimension $D = 3$). The unusual transition was observed in the low fields: the behavior with an applied field decreasing from the medium fields (80 ÷ 2000 kA/m) to low fields (5 ÷ 25 kA/m) reveals the power-law transition from one with exponent $n = -1/2$ to that $n = -1$. The observed power law $\delta M(H)/M_S \propto H^{-1}$ is assumed to be corresponded to the anisotropic magnetic correlation volumes V_H (dimension $D = 2$). The structural correlation length L_C were estimated by the correlation magnetometry and it is about 9 interatomic distances. For the studied amorphous Fe-Cu-Nb-Si-B ribbons, L_C in order of magnitude is close to the value of a coherent scattering length estimated from the X-ray diffraction peak width.

CRediT authorship contribution statement

N.V. Ilin: Conceptualization, Software, Formal analysis, Investigation, Writing – original draft, Visualization. **S.V. Komogortsev:** Conceptualization, Data curation, Writing – review & editing, Supervision, Methodology, Validation. **G.S. Kraynova:** Resources, Writing – review & editing. **A.V. Davydenko:** Investigation, Resources. **I.A. Tkachenko:** Investigation, Resources. **A.G. Kozlov:** Resources. **V.V. Tkachev:** Investigation, Resources. **V.S. Plotnikov:** Resources, Supervision, Project administration.

Declaration of Competing Interest

The authors declare that they have no known competing financial interests or personal relationships that could have appeared to influence the work reported in this paper.

Acknowledgements

The reported study was funded by RFBR, project number 19-32-

90182, and by the state task of the Ministry of Science and Higher Education of the Russian Federation №0657-2020-0005. The measurements carried out using the Kerr-microscope were funded by the state task of the Ministry of Science and Higher Education of the Russian Federation №0657-2020-0013.

References

[1] J.M. Silveyra, E. Ferrara, D.L. Huber, T.C. Monson, Soft magnetic materials for a sustainable and electrified world, Science (80-.). 362 (2018) eaao0195. 10.1126/science.aao0195.
[2] E.A. Périgo, B. Weidenfeller, P. Kollár, J. Füzer, Past, present, and future of soft magnetic composites, Appl. Phys. Rev. 5 (2018), 031301, https://doi.org/10.1063/1.5027045.
[3] R. Alben, J.J. Becker, M.C. Chi, Random anisotropy in amorphous ferromagnets, J. Appl. Phys. 49 (3) (1978) 1653–1658, https://doi.org/10.1063/1.324881.
[4] G. Herzer, Modern soft magnets: Amorphous and nanocrystalline materials, Acta Mater. 61 (3) (2013) 718–734, https://doi.org/10.1016/j.actamat.2012.10.040.
[5] M.A. Willard, M. Daniil, Nanocrystalline Soft Magnetic Alloys Two Decades of Progress, in: K.H.J. Buschow (Ed.), Handb. Magn. Mater., North Holland, 2013: pp. 173–342. 10.1016/B978-0-444-59593-5.00004-0.
[6] R.S. Iskhakov, S.V. Komogortsev, Magnetic microstructure of amorphous, nanocrystalline, and nanophase ferromagnets, Phys. Met. Metallogr. 112 (7) (2011) 666–681, https://doi.org/10.1134/S0031918X11070064.
[7] J. Echigoya, R. Yue, Grain-size dependence of coercive force in sputtered and annealed iron films, J. Mater. Sci. 40 (12) (2005) 3209–3212, https://doi.org/10.1007/s10853-005-2686-0.
[8] O. Kohmoto, N. Uchida, E. Aoyagi, T. Choh, K. Hiraga, Magnetic domain structures of rapidly quenched Fe-Cu-Nb-Si-B alloys observed by Lorentz microscopy, Mater. Trans. JIM. 31 (1990) 820–823, https://doi.org/10.2320/matertrans1989.31.820.
[9] S.V. Komogortsev, R.S. Iskhakov, E.N. Sheftel, E.V. Harin, A.I. Krikunov, E. V. Eremin, Magnetization correlations and random magnetic anisotropy in nanocrystalline films Fe78Zr10N12, Solid State Phenom. 190 (2012) 486–489, https://doi.org/10.4028/www.scientific.net/SSP.190.486.
[10] S. Mühlbauer, D. Honecker, É.A. Périgo, F. Bergner, S. Disch, A. Heinemann, S. Erokhin, D. Berkov, C. Leighton, M.R. Eskildsen, A. Michels, Magnetic small-angle neutron scattering, Rev. Mod. Phys. 91 (2019), 015004, https://doi.org/10.1103/RevModPhys.91.015004.
[11] R.S. Iskhakov, V.A. Ignatchenko, S.V. Komogortsev, A.D. Balaev, Study of magnetic correlations in nanostructured ferromagnets by correlation magnetometry, J. Exp. Theor. Phys. Lett. 78 (10) (2003) 646–650, https://doi.org/10.1134/1.1644310.
[12] V.A. Ignatchenko, R.S. Iskhakov, G.V. Popov, Law of approach of the magnetization to saturation in amorphous ferromagnets, Sov. Phys. JETP 55 (1982) 878–886. http://www.jetp.ac.ru/cgi-bin/dn/e_055_05_0878.pdf.
[13] E.M. Chudnovsky, Magnetic properties of amorphous ferromagnets (invited), J. Appl. Phys. 64 (10) (1988) 5770–5775, https://doi.org/10.1063/1.342227.
[14] E.M. Chudnovsky, Dependence of the magnetization law on structural disorder in amorphous ferromagnets, J. Magn. Magn. Mater. 79 (1) (1989) 127–130, https://doi.org/10.1016/0304-8853(89)90302-8.
[15] V.A. Ignatchenko, R.S. Iskhakov, Magnetization curve of ferromagnets with anisotropic and low-dimension heterogeneities, Fiz. Met. I Metalloved. 6 (1992) 75–86.
[16] Y. Yoshizawa, S. Oguma, K. Yamauchi, New Fe-based soft magnetic alloys composed of ultrafine grain structure, J. Appl. Phys. 64 (10) (1988) 6044–6046, https://doi.org/10.1063/1.342149.
[17] Y. Yoshizawa, Magnetic Properties and Microstructure of Nanocrystalline Fe-Based Alloys, Mater. Sci. Forum. 307 (1999) 51–62, https://doi.org/10.4028/www.scientific.net/MSF.307.51.
[18] J.M.D. Coey, Magnetism and Magnetic Materials, Cambridge University Press, New York, 2010 https://www.cambridge.org/core/product/identifier/9780511845000/type/book.
[19] J. Tejada, B. Martinez, A. Labarta, E.M. Chudnovsky, Correlated spin glass generated by structural disorder in the amorphous Dy6Fe74B20 alloy, Phys. Rev. B 44 (1991) 7698–7700, https://doi.org/10.1103/PhysRevB.44.7698.
[20] C. Herring, R.M. Bozorth, A.E. Clark, T.R. McGuire, High-Field Susceptibilities of Iron and Nickel, J. Appl. Phys. 37 (3) (1966) 1340–1341, https://doi.org/10.1063/1.1708462.
[21] R. Pauthenet, Experimental verification of spin-wave theory in high fields (invited), J. Appl. Phys. 53 (11) (1982) 8187–8192, https://doi.org/10.1063/1.330287.
[22] H. Kronmüller, M. Fähnle, M. Domann, H. Grimm, R. Grimm, B. Gröger, Magnetic properties of amorphous ferromagnetic alloys, J. Magn. Magn. Mater. 13 (1-2) (1979) 53–70, https://doi.org/10.1016/0304-8853(79)90029-5.
[23] H. Kronmuller, Micromagnetism in Amorphous Alloys, IEEE Trans. Magn. 15 (5) (1979) 1218–1225, https://doi.org/10.1109/TMAG.1979.1060343.
[24] S.V. Komogortsev, R.S. Iskhakov, V.A. Fel'k, Fractal dimension effect on the magnetization curves of exchange-coupled clusters of magnetic nanoparticles, J. Exp. Theor. Phys. 128 (2019) 754–760, https://doi.org/10.1134/S1063776119040095.
[25] B. Barbara, V.S. Amaral, J. Filippi, Quantitative description of the magnetization curves of amorphous alloys of the series a-DyxGd1−xNi, J. Magn. Magn. Mater. 116 (1-2) (1992) 58–60, https://doi.org/10.1016/0304-8853(92)90137-D.
[26] W.A. Bryden, J.S. Morgan, T.J. Kistenmacher, K. Moorjani, Correlation of electrical transport and magnetism in amorphous Mn-B alloys, J. Appl. Phys. 61 (8) (1987) 3661–3663, https://doi.org/10.1063/1.338680.
[27] C. Binns, M.J. Maher, Magnetic behaviour of thin films produced by depositing pre-formed Fe and Co nanoclusters, New J. Phys. 4 (2002) 85, https://doi.org/10.1088/1367-2630/4/1/385.
[28] P. Garoche, A.P. Malozemoff, Approach to magnetic saturation in sputtered amorphous films: Effects of structural defects, microscopic anisotropy, and surface roughness, Phys. Rev. B 29 (1984) 226–231, https://doi.org/10.1103/PhysRevB.29.226.
[29] R. Skomski, Nanomagnetics, J. Phys. Condens. Matter. 15 (20) (2003) R841–R896, https://doi.org/10.1088/0953-8984/15/20/202.
[30] A.L. Patterson, The Scherrer formula for X-ray particle size determination, Phys. Rev. 56 (10) (1939) 978–982, https://doi.org/10.1103/PhysRev.56.978.
[31] C. Kittel, Introduction to Solid State Physics, 8th ed., Wiley, New York, 2004.
[32] F. Keffer, Spin Waves, in: H.P.J. Wijn (Ed.), Springer, Berlin, Heidelberg, 1966: pp. 1–273. 10.1007/978-3-642-46035-7_1.
[33] S.V. Komogortsev, G.S. Krainova, N.V. Il'in, V.S. Plotnikov, L.A. Chekanova, I. V. Nemtsev, G.Yu. Yurkin, R.S. Iskhakov, D.A. Yatmanov, Features of the Ferromagnetic Resonance of Amorphous FeSiBNbCu Ribbons with Different Compositions, Inorg. Mater. Appl. Res. 11 (1) (2020) 177–180, https://doi.org/10.1134/S2075113320010219.
[34] A. Hubert, R. Schäfer, Magnetic Domains, Springer Berlin Heidelberg, Berlin, Heidelberg, 1998. 10.1007/978-3-540-85054-0.
[35] R. Schäfer, Domains in 'extremely' soft magnetic materials, J. Magn. Magn. Mater. 215–216 (2000) 652–663, https://doi.org/10.1016/S0304-8853(00)00252-3.
[36] H. Kronmüller, B. Gröger, Domains, domain walls and the coercive field of amorphous ferromagnets, J. Phys. 42 (9) (1981) 1285–1292, https://doi.org/10.1051/jphys:019810042090128500.
[37] Y. Obi, H. Fujimori, H. Saito, Magnetic domain structure of an amorphous Fe-P-C Alloy, Jpn. J. Appl. Phys. 15 (4) (1976) 611–617, https://doi.org/10.1143/JJAP.15.611.
[38] L.P. Tarasov, Ferromagnetic anisotropy of iron and iron-rich silicon alloys, Phys. Rev. 56 (12) (1939) 1231–1240, https://doi.org/10.1103/PhysRev.56.1231.
[39] B.D. Cullity, C.D. Graham, Introduction to Magnetic Materials, John Wiley & Sons, Inc., Hoboken, NJ, USA, 2008. 10.1002/9780470386323.
[40] A. El Boubekri, M. Ounacer, M. Sajieddine, M. Sahlaoui, H. Lassri, R. Moubah, E. K. Hlil, A. Razouk, E. Agouriane, Effects of Cr substitution on the low temperature magnetization behavior in amorphous Fe68+Cr12-Si8B12 ribbons, J. Non. Cryst. Solids 551 (2021), 120437, https://doi.org/10.1016/j.jnoncrysol.2020.120437.
[41] H. Lassri, O. Msieh, O. Touraghe, Z. Yamkane, N. Omari, L. Bessais, Random anisotropy studies in amorphous Co–Er–B ribbons, J. Non. Cryst. Solids 357 (1) (2011) 28–30, https://doi.org/10.1016/j.jnoncrysol.2010.10.005.
[42] R.S. Iskhakov, S.V. Komogortsev, Zh.M. Moroz, E.E. Shalygina, Characteristics of the magnetic microstructure of amorphous and nanocrystalline ferromagnets with a random anisotropy: Theoretical estimates and experiment, J. Exp. Theor. Phys. Lett. 72 (12) (2000) 603–607, https://doi.org/10.1134/1.1351199.
[43] S.V. Komogortsev, R.S. Iskhakov, Law of approach to magnetic saturation in nanocrystalline and amorphous ferromagnets with improved transition behavior between power-law regimes, J. Magn. Magn. Mater. 440 (2017) 213–216, https://doi.org/10.1016/j.jmmm.2016.12.145.
[44] E.N. Sheftel, E.V. Harin, Two modes of magnetic structure of nanocrystalline FeZrN films prepared by oblique-angle magnetron sputtering, J. Magn. Magn. Mater. 479 (2019) 84–87, https://doi.org/10.1016/j.jmmm.2019.02.027.
[45] E.V. Harin, E.N. Sheftel, V.A. Tedzhetov, G.S. Usmanova, Two-Mode Stochastic Magnetic Structure in Nanocrystalline Soft Magnetic Fe–Zr Films, Phys. Status Solidi. 256 (2019) 1900067, https://doi.org/10.1002/pssb.201900067.
[46] R.S. Iskhakov, S.V. Komogortsev, A.D. Balaev, A.A. Gavriliuk, The manifestations of the two-dimensional magnetic correlations in the nanocrystalline ribbons Fe64Co21B15, J. Magn. Magn. Mater. 374 (2015) 423–426, https://doi.org/10.1016/j.jmmm.2014.08.078.
[47] A.K. Singh (Ed.), Advanced X-ray Techniques in Research and Industry, IOS Press, Washington, 2005.